
Dynamic Graph Message Passing Networks

Li Zhang

Department of Engineering Science
University of Oxford
lz@robots.ox.ac.uk

Dan Xu

Department of Engineering Science
University of Oxford
danxu@robots.ox.ac.uk

Anurag Arnab

Department of Engineering Science
University of Oxford
aarnab@robots.ox.ac.uk

Philip H.S. Torr

Department of Engineering Science
University of Oxford
phst@robots.ox.ac.uk

Abstract

Modelling long-range dependencies is critical for complex scene understanding tasks such as semantic segmentation and object detection. Although CNNs have excelled in many computer vision tasks, they are still limited in capturing long-range structured relationships as they typically consist of layers of local kernels. A fully-connected graph is beneficial for such modelling, however, its computational overhead is prohibitive. We propose a dynamic graph message passing network, based on the *message passing neural network* framework [16], that significantly reduces the computational complexity compared to related works modelling a fully-connected graph. This is achieved by adaptively sampling nodes in the graph, conditioned on the input, for message passing. Based on the sampled nodes, we then dynamically predict node-dependent filter weights and the affinity matrix for propagating information between them. Using this model, we show significant improvements with respect to strong, state-of-the-art baselines on three different tasks and backbone architectures. Our approach also outperforms fully-connected graphs while using substantially fewer floating point operations and parameters.

1 Introduction

Capturing long-range dependencies is crucial for complex scene understanding tasks such as semantic segmentation, instance segmentation and object detection. Although convolutional neural networks (CNNs) have excelled in a wide range of scene understanding tasks [27, 44, 19], they are still limited by their ability to capture these long-range interactions. Several techniques have been proposed in the literature to improve the capability of CNNs to capture long-range context, such as dilated convolutions [6, 55], incorporating Conditional Random Fields (CRFs) into deep networks [6, 60, 51] and attention-based models [46, 1, 45].

Non-local networks [48] are a popular generalisation of the attention model of [46] to computer vision tasks. It learns pairwise structured relationships among all feature elements in a feature map to produce the attention weights which are used for feature aggregation. Considering each feature element as a node in a graph, Non-local networks effectively model a fully-connected feature graph and thus have a quadratic inference complexity with respect to the number of the feature elements. This is infeasible for dense prediction tasks on high-resolution imagery, as commonly encountered in semantic segmentation [12]. Moreover, in dense prediction tasks, capturing relations between all pairs of pixels is usually unnecessary due to the redundant information contained within the image (Fig. 1). Simply subsampling the feature map to reduce the memory requirements is also suboptimal, as such naïve subsampling would result in smaller objects in the image not being represented adequately.



Figure 1: Contextual information is crucial for complex scene understanding tasks. To recognise the “boathouse”, one needs to consider the “boat” and the “water” next to it. Fully-connected message passing models (a) are able to obtain this information, but are prohibitively expensive. Furthermore, they capture a lot of redundant information (*i.e.* “trees” and “sky”). Locally-connected models (b) are more efficient, but miss out on important context. Our proposed approach (c), dynamically samples a small subset of relevant feature nodes based on a *learned* sampling scheme, *i.e.* the *learned* random walk (indicated by the white dashed arrow lines), and also dynamically predicts filter weights (indicated by unique node colours) and affinities (indicated by unique edge colours), which are both conditioned on the sampled feature nodes.

Graph convolution networks (GCNs) [25, 16], which propagate information along graph-structured input data, can alleviate the computational issues of Non-local networks to a certain extent. However, this stands only if local neighbourhoods are considered for each node. Employing such local-connected graphs means that the long-range contextual information needed for complex vision tasks such as segmentation and detection [37, 35] will only be partially captured. Furthermore, the modelling capacity of GCNs are also restricted as they commonly assume a static input graph where the neighbours for each node are fixed and the filter weights are shared among all nodes.

To address the aforementioned issues, we propose a novel dynamic graph message passing network (DGMN) model for deep representational learning, based on the general message-passing neural network [16] framework. The proposed model has two key dynamic properties (see Fig. 1): Firstly, it dynamically samples the neighbourhood of a node conditioned on the input. Intuitively, this allows the network to efficiently gather long-range context by only selecting a subset of the most relevant nodes in the graph; Secondly, based on the nodes that have been sampled, we further dynamically predict node-conditioned filter weights and the affinity matrix, which are used to propagate information among the feature nodes via message passing. The dynamic weights and affinities are especially beneficial for us to specifically model each sampled feature context, thus leading to more effective message passing. Both of these dynamic properties are jointly optimised in a single model, and the whole DGMN is modularised as a network layer for simple deployment in any backbone architecture.

We demonstrate the proposed model on the tasks of semantic segmentation, object detection and instance segmentation on the challenging Cityscapes [12] and COCO [32] datasets. We achieve better performance than the fully-connected Non-local model [48], while using substantially fewer floating point operations (FLOPs) and parameters. Significantly, one variant of our model with dynamic filters and affinities (*i.e.* the second dynamic property) achieves similar performance to Non-local while only using 9.4% of its FLOPs and 25.3% of its parameters. Furthermore, “plugging” our module into existing networks, we show considerable improvements with respect to strong, state-of-the-art baselines on three different tasks and backbone architectures.

2 Related Work

An early technique for increasing the receptive field of CNNs was to use dilated or atrous convolutions. With dilated convolutions [6, 55], the number of parameters does not change, while the receptive field grows exponentially if the dilation rate is linearly increased in successive layers. Other modifications to the convolution operation include deformable convolutions [14, 61], which learn the offset with

respect to a predefined grid with which to select input values. However, the weights of the deformable convolution filters are still shared across different positions, and are not conditioned on the input.

Another popular paradigm for deep representation learning has been graph neural networks (GNNs), which aim to propagate information throughout a graph, and were originally designed for graph structured input data [39, 25, 33]. A number of different GNN architectures have been developed for image domains for the purpose of feature learning [43, 20, 48], since images can also be considered as structured graphs where each pixel is connected to its neighbours. This is also the focus of this work. Although Non-local [48] does not explicitly model a graph, it learns a full affinity map describing the structured relationship between each pair of feature nodes, and thus it effectively learns a fully-connected graph representation. There are also works that adapt Non-local to the task of semantic segmentation [56, 21]. In this paper, we consider message passing neural networks (MPNN) [16] which consist of a message passing and a readout phase, and generalise different graph neural network approaches [25, 5, 2, 30, 3, 40]. Different from existing works considering either a static and/or a fully-connected graph, our model explores a dynamic graph which simultaneously learns dynamic node sampling, and predicts dynamic filters and affinities in a unified deep model. GraphSAGE [17] is also a graph-based method using a sampling strategy for feature embedding, however, their nodes are sampled simply based on the spatial distribution of the nodes, and a uniform sampling strategy is considered in their approach. In contrast, our sampling strategy is learned with the network optimisation and conditioned on the node features. GraphSAGE also did not consider another dynamic property, *i.e.* dynamic prediction of the affinities and the message passing kernels.

Jia *et al.* [23] develop an idea of “dynamic filter/convolution”, predicting a dynamic convolutional filter for each position, where the weights of the filters are not shared spatially. A recently published approach [49] further reduce the complexity of the dynamic convolutional operation for natural language processing with lightweight group convolutions. Shelhamer *et al.* [41] parameterised convolutional filters as a composition of jointly learned Gaussian filters and standard, “free-form” filters. These models essentially learn the dynamic affinities in our model when they tie the *normalised* weights of all channels. More importantly, unlike [23, 49, 41], we present a graph-based formulation, and jointly learn dynamic weights and dynamic affinities, which are conditioned on an *adaptively sampled* neighbourhood of each feature node in the graph using the proposed dynamic sampling strategy for effective message passing. Our model also experimentally shows clear improvements over these methods on multiple tasks.

3 Dynamic Graph Message Passing Networks

3.1 Problem Definition and Notation

Given an input observation deep feature map interpreted as a set of feature vectors, *i.e.* $\mathbf{F} = \{\mathbf{f}_i\}_{i=1}^N$ with $\mathbf{f}_i \in \mathbb{R}^{1 \times C}$, where N is the number of pixels and C is the feature dimension respectively, our goal is to learn a set of refined latent feature vectors $\mathbf{H} = \{\mathbf{h}_i\}_{i=1}^N$ via utilising hidden structured information among the feature vectors at different pixel locations. \mathbf{H} has the same dimension as the observation \mathbf{F} . To learn such structured representations, we convert the feature map into a graph domain by constructing a feature graph $\mathcal{G} = \{\mathcal{V}, \mathcal{E}, A\}$ with \mathcal{V} as its nodes, \mathcal{E} as its edges and A as its adjacency matrix. Specifically, the nodes of the graph are represented by the latent feature vectors, *i.e.* $\mathcal{V} = \{\mathbf{h}_i\}_{i=1}^N$, and $A \in \mathbb{R}^{N \times N}$ is a binary or learnable matrix with self-loops describing the connections between nodes. In this work, we propose a novel dynamic graph message passing network for deep representation learning, which refines each graph feature node by passing messages on the graph \mathcal{G} . Different from existing message passing neural networks considering a fully- or locally-connected static graph [48, 16], we propose a dynamic graph network model with two dynamic properties, *i.e.* dynamic sampling of graph nodes to approximate the full graph distribution, and dynamic prediction of node-conditioned filter weights and affinities, in order to achieve more efficient and effective message passing.

3.2 Graph Message Passing Neural Networks for Deep Representation Learning

Message passing neural networks (MPNNs) [16] present a generalised form of graph neural networks such as graph convolution networks [25], gated graph sequential networks [30] and graph attention networks [47]. In order to model structured graph data, in which the latent variables are represented as nodes on an undirected or directed graph, feed-forward inference is performed through a message

passing phase followed by a readout phase upon the graph nodes. The message passing phase usually takes T iteration steps to update feature nodes, while the readout phase is for the network prediction *e.g.* graph classification with updated nodes. In this work, we focus on the message passing phase for learning efficient and effective feature refinement, since well-represented features are critical in all downstream tasks. The message passing phase consists of two steps, *i.e.* a message calculation step M^t and a message updating step U^t . Given a latent feature node $\mathbf{h}_i^{(t)}$ at an iteration step t , for computational efficiency, we consider a locally connected node field with $v_i \subset \mathcal{V}$ and $v_i \in \mathbb{R}^{(K \times C)}$, where $K \ll N$ is the number of sampled nodes in v_i . Thus we can define the message calculation step for node i operated locally as follows:

$$\mathbf{m}_i^{(t+1)} = M^t \left(A_{i,j}, \{\mathbf{h}_1^{(t)}, \dots, \mathbf{h}_K^{(t)}\}, \mathbf{w}_j \right) = \sum_{j \in \mathcal{N}(i)} A_{i,j} \mathbf{h}_j^{(t)} \mathbf{w}_j, \text{ with } A_{i,j} = A[i, j], \quad (1)$$

where $A_{i,j}$ describes the connection relationship *i.e.* the affinity between latent nodes $\mathbf{h}_i^{(t)}$ and $\mathbf{h}_j^{(t)}$, $\mathcal{N}(i)$ denotes a self-included neighborhood of the node $\mathbf{h}_i^{(t)}$ which can be derived from v_i , $\mathbf{w}_j \in \mathbb{R}^{C \times C}$ is a transformation matrix for message calculation on the hidden node $\mathbf{h}_j^{(t)}$. Then the message updating function U^t is applied to update the node $\mathbf{h}_i^{(t)}$ with a linear combination of the calculated message and the observation feature \mathbf{f}_i at the node position i as:

$$\mathbf{h}_i^{(t+1)} = U^t \left(\mathbf{f}_i, \mathbf{m}_i^{(t+1)} \right) = \sigma \left(\mathbf{f}_i + \alpha_i^m \mathbf{m}_i^{(t+1)} \right), \quad (2)$$

where α_i^m of a learnable parameter for scaling the message, and the operation $\sigma(\cdot)$ is a non-linearity function *e.g.* ReLU. By iteratively performing message passing on each node with T steps, we obtain a refined feature map $\mathbf{H}^{(T)}$ as output.

3.3 From Fully-Connected Graph to Dynamic Sampling Graph

A fully-connected graph typically contains many connections and parameters, which thus naturally brings redundancy in the connections, and also makes the network optimisation more difficult especially when we deal with limited training data. Therefore, as in Eq. 1, a local node connection field is considered in the graph message passing network, in order to substantially reduce the computational overhead of large fully-connected graphs. However, in various computer vision tasks, such as detection and segmentation, learning deep representations capturing both local and global receptive fields is important for the model performance [37, 35]. To maintain a large receptive field while utilising much fewer parameters than the fully-connected setting, we further explore dynamic sampling strategies in the proposed graph message passing network. A uniform sampling scheme and a predicted random walk sampling scheme are developed aiming to effectively reduce the redundancy in the fully-connected graph. The sampling is performed in a dynamic fashion, meaning that for a given node \mathbf{h}_i , we aim to sample an optimal subset of v_i from \mathcal{V} to update \mathbf{h}_i via message passing.

Uniform sampling for dynamic receptive fields. Uniform sampling is a commonly used strategy for graph node sampling [28] based on Monte-Carlo estimation. To approximate the distribution of \mathcal{V} , we consider a set of S uniform sampling rates φ with $\varphi = \{\rho_q\}_{q=1}^S$, where ρ_q is a sampling rate. Let us assume that the latent feature nodes are located in a P -dimensional space \mathbb{R}^P . For instance, P equals to 2 for images considering the x - and y -dimension on the image plane. For each latent node \mathbf{h}_i , a total of K neighbouring nodes are sampled from \mathbb{R}^P . The receptive field of v_i is thus determined by ρ_q and K . Note that since $S, K \ll N$, and $S * K \ll N$, we are able to capture a wide range of the receptive fields while maintaining a small number of connected nodes. Thus we can achieve much lower computational overhead compared with fully-connected message passing in which typically all N nodes are used when one of the nodes is updated. Each node receives S complementary messages from distinct receptive fields for updating as follows:

$$\mathbf{m}_i^{(t+1)} = \sum_q \sum_{j \in \mathcal{N}_q(i)} \beta_q A_{i,j}^q \mathbf{h}_j^{(t)} \mathbf{w}_j^q, \text{ with } A_{i,j}^q = A^q[i, j] \text{ and } q = 1, \dots, S \quad (3)$$

where β_q is a weighting parameter for the message from the q -th sampling rate. A^q denotes a formed adjacent matrix under a sampling rate ρ_q , with $A_{i,j}^q$, \mathbf{w}_j^q and $\mathcal{N}_q(i)$ defined analogously. The uniform sampling scheme acts as a linear sampler based on spatial distribution while not considering the

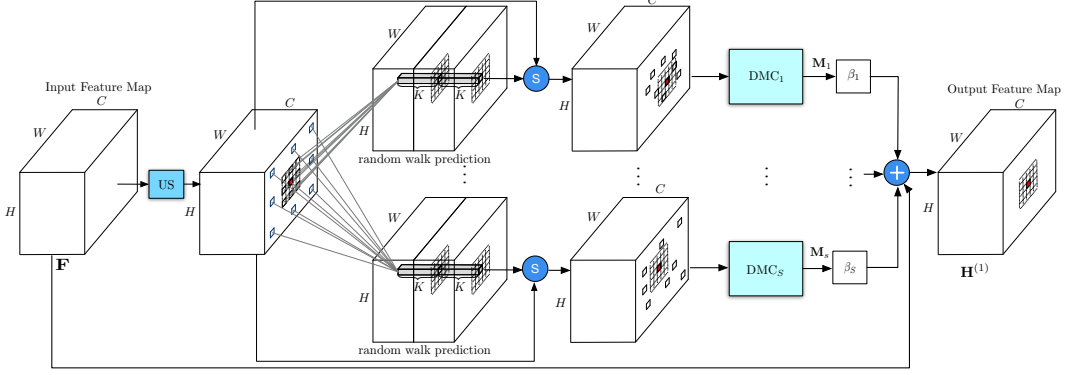


Figure 2: Schematic illustration of the overall proposed dynamic graph message passing network (DGMN) model. ‘US’ denotes the uniform sampling operation with a set of S neighbourhoods for each current receiving feature node (red square). Each neighbourhood contains K (e.g. 3×3) sampled nodes. The symbol \textcircled{S} represents the random walk sampling operation based on the position specific and feature dependant random walk prediction. $\text{DMC}_1, \dots, \text{DMC}_S$ and β_1, \dots, β_S denotes S dynamic message calculation modules and S message scaling parameters, respectively. The DMC module is detailed in Figure 3. The symbol \oplus indicates an element-wise addition operation.

original feature distribution of the hidden nodes, *i.e.* sampling not dependant on the node features. Eq. 2 can still be used to update the nodes.

Random walks for non-linear adaptive sampling. To take into account the feature data distribution when sampling nodes, we further present a random walk strategy upon the uniform sampling. Walks around the uniformly sampled nodes could sample the graph in a non-linear and adaptive manner, and we believe that it could facilitate learning better approximation of the original feature distribution. Figure 4 shows that the nodes are adaptively sampled which semantically captures the objects’ scale and shape. The “random” here refers to the fact that the walks are predicted in a data-driven fashion from stochastic gradient descent. Given a set of uniformly sampled nodes $v_i^q \in \mathbb{R}^{K \times C}$ under a sampling rate ρ_q , the random walk of each node is further estimated based on the feature data of the sampled node set. Given the P -dimensional space where the nodes distribute ($P = 2$ in Figure 2 for considering the x - and y -dimension on the image plane), let us denote $\Delta \mathbf{d}_j^q \in \mathbb{R}^{P \times 1}$ as predicted walks from a uniformly sampled node \mathbf{h}_j with $j \in \mathcal{N}_q(i)$. The node walk prediction can then be performed using a matrix transformation written as:

$$\Delta \mathbf{d}_j^q = \mathbf{W}_{i,j}^q v_i^q + \mathbf{b}_{i,j}^q, \quad (4)$$

where $\mathbf{W}_{i,j}^q \in \mathbb{R}^{P \times (K \times C)}$ and $\mathbf{b}_{i,j}^q \in \mathbb{R}^{P \times 1}$ are the matrix transformation parameters, which are learned separately for each node v_i^q . With the predicted walks, we can obtain a new set of adaptively sampled nodes $v_i^{\prime q}$, and generate the corresponding adjacent matrix $A^{\prime q}$, which can be used to calculate the messages as:

$$\mathbf{m}_i^{(t+1)} = \sum_q \sum_{j \in \mathcal{N}_q(i)} \beta_q A_{i,j}^{\prime q} \varrho \left(\mathbf{h}_j^{\prime (t)} | \mathcal{V}, j, \Delta \mathbf{d}_j^q \right) \mathbf{w}_j^q, \quad \text{with } A_{i,j}^{\prime q} = A^{\prime q}[i, j], \quad (5)$$

where the function $\varrho(\cdot)$ is a bilinear sampler [22] which samples a new feature node $\mathbf{h}_j^{\prime (t)}$ around $\mathbf{h}_j^{(t)}$ given the predicted walk $\Delta \mathbf{d}_j^q$ and the whole set of graph vertexes \mathcal{V} .

3.4 Joint Learning of Node-Conditioned Dynamic Filters and Affinities

In the message calculation formulated in Eq. 5, the set of weights $\{\mathbf{w}_j^q\}_{j=1}^K$ of the filter is shared for each adaptively sampled node field $v_i^{\prime q}$. However, since each $v_i^{\prime q}$ essentially defines a node-specific local feature context, it is more meaningful to use a node-conditioned filter to learn the message for each hidden node $\mathbf{h}_i^{(t)}$. In addition to the filters for the message calculation in Eq. 5, the affinity $A_{i,j}^{\prime}$ of any pair of nodes $\mathbf{h}_i^{\prime (t)}$ and $\mathbf{h}_j^{(t)}$ could be also be predicted and should also be conditioned on the node field $v_i^{\prime q}$, since the affinity reweights the message passing only in $v_i^{\prime q}$. We are then able

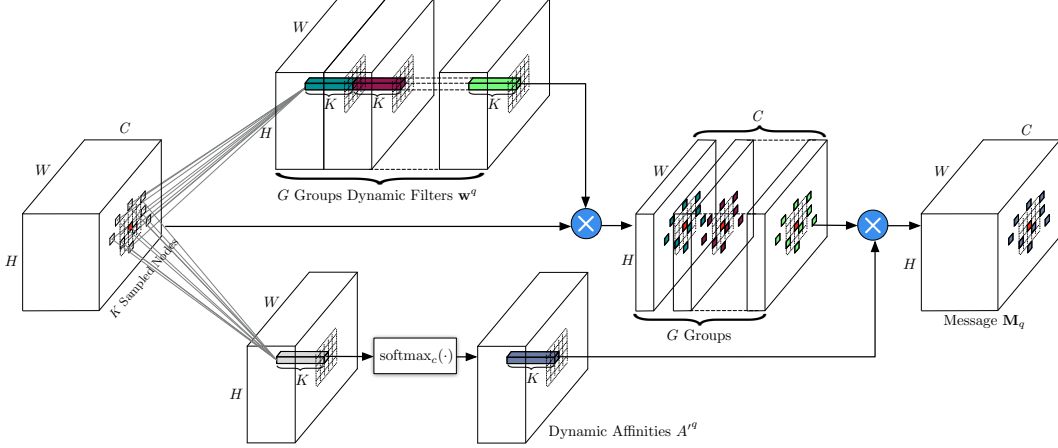


Figure 3: Schematic illustration of the proposed dynamic message passing calculation (DMC) module. The small red square indicates the receiving node whose message is calculated from its neighbourhood, *i.e.* the sampled K (*e.g.* 3×3) features nodes. The module accepts a feature map as input and produces its corresponding message map. The symbol \otimes denotes a matrix multiplication operation using the dynamically predicted and position specific group kernels and affinities.

to use matrix transformation to simultaneously estimate the dynamic filter and affinity which are both conditioned on v_i^q as follows (see Figure 3):

$$\{\mathbf{w}_j^q, A'_{i,j}^q\} = \mathbf{W}_{i,j}^{k,A} v_i^q + \mathbf{b}_{i,j}^{k,A}, \quad (6)$$

$$A'_{i,j}^q = \text{softmax}_c(A'_{i,j}^q) = \frac{\exp(A'_{i,j}^q)}{\sum_{l \in \mathcal{N}_q(i)} \exp(A'_{i,l}^q)}, \quad (7)$$

where the function $\text{softmax}_c(\cdot)$ denotes a softmax operation along the channel axis, which is used to perform a normalisation on the estimated affinity $A'_{i,j}^q \in \mathbb{R}^1$. $\mathbf{W}_{i,j}^{k,A} \in \mathbb{R}^{(G \times C + 1) \times (K \times C)}$ and $\mathbf{b}_{i,j}^{k,A} \in \mathbb{R}^{(G \times C + 1)}$ are matrix transformation parameters. To reduce the number of the filter parameters, we consider using the group transformation [11] with a set of G groups split from the total C feature channels, and $G \ll C$, *i.e.* each group of C/G feature channels shares the same set of filter parameters. For the dynamic weights, we relax them in the prediction without using non-linearity after the matrix transformation. The predicted dynamic filter weights and the affinities are used in Eq. 5 for dynamic message calculation.

Dynamic weights have also been explored recently in [49] for natural language processing. However, [49] is not formulated in a graph model. Moreover, when Wu *et al.* [49] use one group for the normalised weights, *i.e.* $G = 1$. In other words, they only effectively predict the affinities in our model and do not simultaneously consider any filters. As our model jointly predicts dynamic filter weights and dynamic affinities from the same set of graph nodes, it is thus a generalisation of [49]. It should be noted that, different from existing methods predicting the weights using shared kernels for all the convolutional positions [4], our predicted affinities and weights for message passing are *position specific* and *dependant* on the dynamic sampled nodes. Therefore our model is able to better capture position based semantic context and thus facilitates dynamical feature message passing.

4 Modular Instantiation

Figure 2 shows how our proposed dynamic graph message passing network (DGMN) can be implemented in neural networks. The proposed module accepts a single feature map \mathbf{F} as input, which can be derived from any CNN layer. $\mathbf{H}^{(0)}$ denotes an initial state of the latent feature map, \mathbf{H} , and is initialised with \mathbf{F} . \mathbf{H} and \mathbf{F} have the same dimension, *i.e.* $\mathbf{F}, \mathbf{H} \in \mathbb{R}^{H \times W \times C}$, where H , W and C are the height, width and the number of feature channels of the feature map respectively. We first define a set of S uniform sampling rate (we show two uniform sampling rate in Figure 2 and omit others). The uniform and the random walk sampler sample the nodes from the full graph

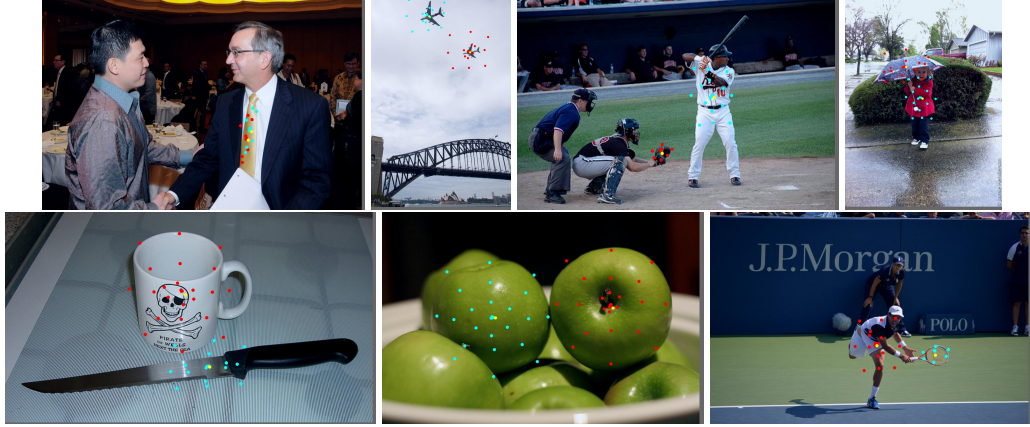


Figure 4: Visualisation of the nodes sampled via *learning* the random walks with our network. The yellow point indicates a receiving node i , and the red or cyan points show the sampled nodes which send messages to it.

and return the node indices for subsequent dynamic message calculation (DMC) in Figure 3. We referred to [14] for the implementation of the random walk prediction in neural networks. The matrix transformation $\mathbf{W}_{i,j}^q$ to estimate the node random walk in Eq 4 is implemented by a 3×3 conv layer. Note that other sampling strategies could also be flexibly employed in our framework. If the random walking sampling is not used, the uniform sampled feature nodes are directly input into dynamic message calculation module (DMC). The sampled feature nodes are processed along two data paths: one for predicting the node-dependent dynamic affinities $A^q \in \mathbb{R}^{H \times W \times K}$ and another path for dynamic filters $\mathbf{w}^q \in \mathbb{R}^{H \times W \times K \times G}$ where K (e.g., 3×3) is the kernel size for the receiving node and we set $G = 4$ for group transformation [11]. The matrix transformation $\mathbf{W}_{i,j}^{k,A}$ used to jointly predict the dynamic filters and affinities in Eq 6 is implemented by a 3×3 conv layer. Message $\mathbf{M}_q \in \mathbb{R}^{H \times W \times C}$ corresponding to the q -th sampling rate is calculated with matrix multiplication and then scaled to perform a linear combination with the observation feature map \mathbf{F} , to produce a refined feature map $\mathbf{H}^{(1)}$ as output. To balance performance and efficiency, as in [31], we perform $T = 1$ iteration of message updating. In the existing popular graph-based feature learning models, such as GloRe [10], they also consider only using $T = 1$ to have a good balance between the performance and the efficiency. We used $T = 1$ for all the experiments, which we find on experimental results already achieves superior performance.

5 Experiments

5.1 Experimental Setup

Datasets. We evaluate our proposed model on two challenging public benchmarks, *i.e.* Cityscapes [12] for semantic segmentation, and COCO [32] for object detection and instance segmentation. Both datasets have hidden test sets which are evaluated on a public evaluation server. *Cityscapes* has densely annotated semantic labels for 19 categories in urban road scenes, and contains a total of 5000 finely annotated images, divided into 2975, 500, and 1525 images for training, validation and testing, respectively. We do not use the coarsely annotated data in our experiments. The images of this dataset have a high resolution of 1024×2048 . Following the standard evaluation protocol [12], the metric of mean Intersection over Union (mIoU) averaged over all classes is used. *COCO 2017* consists of 80 object classes with a training set of 118,000 images, a validation set of 5000 images, and a test set of 2000 images. We follow the standard COCO evaluation metrics [32, 18] to evaluate the performance of object detection and instance segmentation, employing the metric of mean average-precision (mAP) at different box and mask IoUs respectively.

Implementation details. For the semantic segmentation task on Cityscapes, we follow [58, 7] and use a polynomial learning rate decay with an initial learning rate of 0.01. The momentum and the weight decay are set to 0.9 and 0.0001 respectively. We use 4 Nvidia V100 GPUs, batch size 8 and run $40k$ iterations for the experiments on Cityscapes training set. For data augmentation, random cropping with a crop size of 769 and random mirror flipping are applied on the fly during training. The backbone network structure consists of a fully convolutional network with dilated convolutions [8, 15, 10], with

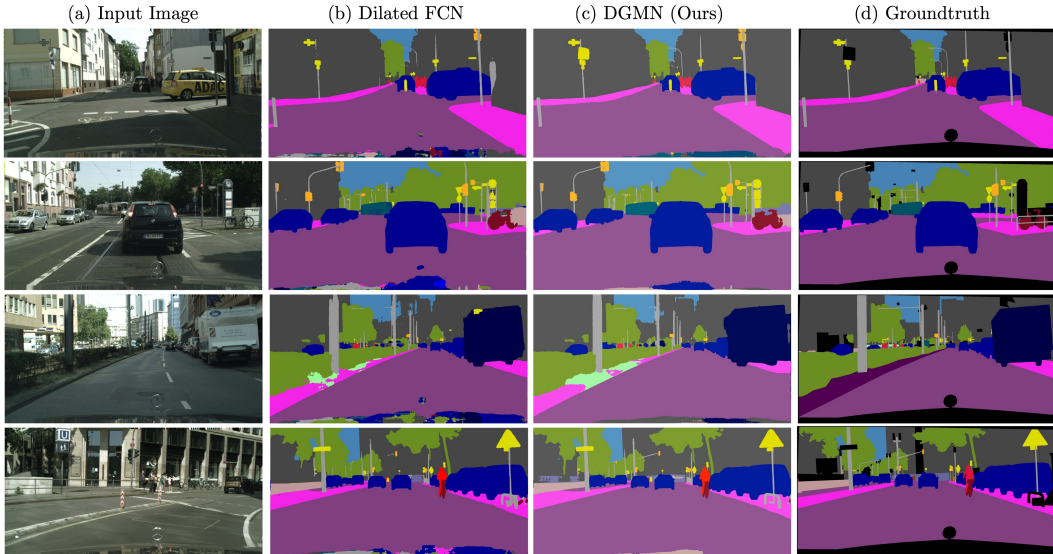


Figure 5: Qualitative results of Dilated FCN baseline [55] and DGMN (ours) on Cityscapes dataset.

Table 1: Quantitative results of different models on the Cityscapes validation set for semantic segmentation. All the methods are evaluated in single-scale mIoU and with a ResNet-101 backbone.

Model	mIoU (%)	Params	FLOPs
Dilated FCN baseline [55]	75.0	–	–
+ Non-local [48]	79.0	+2.88M	+73.33G
+ DGMN Base	75.4	+0.54M	+4.97G
+ DGMN w/ DA	76.5	+0.57M	+5.32G
+ DGMN w/ DA+DW	79.1	+0.73M	+6.88G
+ DGMN w/ DA+US	79.6	+1.78M	+16.75G
+ DGMN w/ DA+RWS	80.2	+2.19M	+20.65G
+ DGMN w/ DA+DW+US	80.3	+2.61M	+24.55G
+ DGMN w/ DA+DW+RWS	80.4	+3.02M	+28.45G

Table 2: State-of-the-art comparison on the Cityscapes test set. All the methods are trained on the fine-annotation training and validation sets.

Method	Backbone	mIoU (%)
SAC [57]	ResNet-101	78.1
DepthSeg [26]	ResNet-101	78.2
BiSeNet [53]	ResNet-101	78.9
AAF [24]	ResNet-101	79.1
DFN [54]	ResNet-101	79.3
PSANet [59]	ResNet-101	80.1
DenseASPP [52]	DenseNet-161	80.6
GloRe [10]	ResNet-101	80.9
DANet [15]	ResNet-101	81.5
OCNet [56]	ResNet-101	81.7
DGMN (Ours)	ResNet-101	81.8

a ResNet-101 front-end pretrained from on ImageNet. A 3×3 convolution layer, together with batch normalisation and ReLU are used after the backbone to produce a dimension-reduced feature map of 512 channels, which is then fed into our proposed module as input. Note that following common practice [58, 56, 59, 38] we used synchronised batch normalisation for better estimation of the batch statistics for the experiments on Cityscapes.

For the tasks of object detection and instance segmentation on COCO, we use the standard configuration of Mask R-CNN [18] with FPN and ResNet/ResNeXt [19, 50] as a backbone architecture. The backbone parameters of all the models in the experiments are pretrained on the ImageNet classification. The input images are resized such that their shorter side is of 800 pixels and the longer side is limited to 1333 pixels. The batch size is set to 16. The initial learning rate is set to 0.02 with a decrease by a factor of 0.1 after 60k and 80k iterations, and finally terminates at 90k iterations. Following [34], the training warm-up is employed by using a smaller learning rate of 0.02×0.3 for the first 500 iterations. All the batch normalisation layers in the backbone are “frozen” during the fine-tuning on COCO. We insert one or multiple random initialised DGMN modules into the backbone for deploying our method. For fair comparison with Non-local [48], we insert one DGMN module right before the last residual block of *res4* (Table 3). Furthermore, we also conduct experiments (Table 4 and 5) by adding DGMN module after all 3×3 layers in *res4* and *res5*. Our models and all baselines are trained with the typical “1x” training settings from the public Mask R-CNN benchmark [34] for all experiments on COCO. We train models on COCO training set only and test on validation set and test-dev set. We use single scale testing for all the evaluations on COCO. For the prediction of the dynamic filter weights, we use the grouping parameter $G = 4$ for all experiments on Cityscapes and COCO.

Table 3: Quantitative results of different models on the COCO 2017 validation set for object detection (AP^{box}) and instance segmentation (AP^{mask}). All methods are based on the Mask R-CNN with ResNet-50 as backbone.

Model	AP^{box}	AP_{50}^{box}	AP_{75}^{box}	AP^{mask}	AP_{50}^{mask}	AP_{75}^{mask}	param	FLOPs
Mask R-CNN baseline [34, 18]	37.8	59.1	41.4	34.4	55.8	36.6	44.13M	279.12G
+ Non-local [48]	38.5	60.0	41.8	34.9	56.5	37.3	+2.10M	+26.52G
+ DGMN w/ DA	38.2	60.0	41.7	34.7	56.4	36.7	+0.68M	+2.81G
+ DGMN w/ DA+US	39.0	60.6	42.6	35.3	57.2	37.6	+0.93M	+3.88G
+ DGMN w/ DA+RWS	39.1	60.8	42.9	35.4	57.3	37.8	+1.10M	+4.57G
+ DGMN w/ DA+DW+RWS	39.5	61.0	43.3	35.7	58.0	37.9	+1.10M	+4.59G

Table 4: Quantitative results of inserting proposed module into multiple layers of the ResNet-50. C4 and C5 denote inserting DGMN after all 3×3 convolutional layers in *res4* and *res5* respectively. Results are presented for object detection and instance segmentation on COCO 2017 validation set.

Model	AP^{box}	AP_{50}^{box}	AP_{75}^{box}	AP^{mask}	AP_{50}^{mask}	AP_{75}^{mask}	Params	FLOPs
Mask R-CNN baseline [34, 18]	37.8	59.1	41.4	34.4	55.8	36.6	44.13M	279.12G
+ DGMN (C5)	40.0	62.0	43.5	36.0	58.5	38.1	+3.48M	+3.57G
+ DGMN (C4, C5)	40.7	62.9	44.4	36.6	59.3	39.1	+6.96M	+17.97G

5.2 Model Analysis

Baseline models. To demonstrate the effectiveness of the proposed DGMN model and analyse the impact of the different components of DGMN on the semantic segmentation and the object detection tasks, we conduct ablation studies considering both Cityscapes and COCO datasets.

For semantic segmentation on Cityscapes, our baseline architecture is Dilated FCN [55], a popular and strong backbone baseline. For object detection and instance segmentation on COCO, our baseline architecture is Mask R-CNN [18] which is another common and strong baseline. Across all tasks and datasets, we consider Non-local networks [48] as an additional baseline. We reimplement Non-local for fair comparison with our model. Note that our reimplementation of Non-local for semantic segmentation on Cityscapes achieves an IoU of 79.0%, outperforming [56] which achieved 78.8%. A qualitative comparison between the Dilated FCN baseline and our DGMN approach is shown in 5.

We denote *DGMN Base* as our basic graph convolutional message passing model (described in Sec. 3.2) with $K = 3 \times 3$. We then add uniform sampling (US), random walk sampling (RWS), dynamic affinities (DA) and dynamic filter weights (DW) upon the DGMN base model. Note that US and RWS were detailed in Sec. 3.3 and DA and DW in Sec. 3.4. For our experiments on Cityscapes, where our network has a stride of 8, the sampling rates are set to $\varphi = \{1, 6, 12, 24, 36\}$. For experiments on COCO, where the network stride is 32, we use smaller sampling rates of $\varphi = \{1, 4, 8, 12\}$. The effect of this hyperparameter is studied in the Appendix A.

Effectiveness of the dynamic sampling strategy. Table 1 shows quantitative results of semantic segmentation on the Cityscapes validation set. DGMN w/ DA+US significantly outperforms DGMN Base and DGMN w/ DA by 4.6 points and 3.1 points respectively. DGMN w/ DA+RWS further improves over DGMN w/ DA+US, meaning that the feature-data driven adaptive sampling based on random walks is more effective than spatial uniform sampling when selecting nodes. Both types of dynamic sampling schemes that we considered achieve superior performance compared with the DGMN base, demonstrating the effectiveness of using dynamic sampling for approximating a fully-connected graph. More importantly, all variants of our module that use dynamic sampling (the last section of Table 1) achieve higher performance than a fully-connected model (*i.e.* Non-local [48]) with substantially fewer FLOPs. This emphasises the performance benefits of our dynamic graph sampling model. Similar trends can also be observed on COCO, for object detection and instance segmentation, as shown in Table 3.

Effectiveness of joint learning the dynamic filters and affinities. As shown in Table 1, DGMN w/ DA is 1.1 points better than DGMN Base with only a slight increase in FLOPs and parameters, showing the benefit of using predicted dynamic affinities for reweighting the messages in message passing. By further employing the estimated dynamic filter weights for message calculation, the performance increases substantially from a mIoU of 76.5% to 79.1%, which is almost the same as



Figure 6: Qualitative examples of the object detection task on the COCO validation dataset. The first and third rows are the results from the Mask R-CNN baseline [34, 18]. The second and fourth row are the detection results from our DGMN approach.

Table 5: Quantitative results via plugging our DGMN module on different backbones on the COCO 2017 test-dev set for object detection (AP^{box}) and instance segmentation (AP^{mask}).

Model	Backbone	AP^{box}	AP_{50}^{box}	AP_{75}^{box}	AP^{mask}	AP_{50}^{mask}	AP_{75}^{mask}
Mask R-CNN [34, 18]	ResNet-50	38.0	59.7	41.5	34.6	56.5	36.6
+ DGMN (C5)		40.2	62.5	43.9	36.2	59.1	38.4
+ DGMN (C4, C5)		41.0	63.2	44.9	36.8	59.8	39.1
Mask R-CNN [34, 18]	ResNet-101	40.2	61.9	44.0	36.2	58.6	38.4
+ DGMN (C5)		41.9	64.1	45.9	37.6	60.9	40.0
Mask R-CNN [34, 18]	ResNeXt-101	42.6	64.9	46.6	38.3	61.6	40.8
+ DGMN (C5)		44.3	66.8	48.4	39.5	63.3	42.1

the 79.2% of the Non-local model [48]. Furthermore, our method only uses 9.4% of the FLOPs and 25.3% of the parameters compared to Non-local. These results clearly demonstrate our motivation of joint learning the dynamic filter weights and dynamic affinities from the same set of graph nodes.

Effectiveness of multiple DGMN modules. In Table 3, we insert our DGMN module right before the last residual block of C4 (*res4*) for fair comparison with Non-local [48]. In this experiment, we further show our module’s ability to learn rich feature representations by inserting multiple proposed modules in backbone ResNet-50. Specifically, Table 4 shows that our final model DGMN (w/ DA+DW+RWS) significantly improved upon the Mask R-CNN baseline by inserting the proposed module in all the residual blocks (after 3×3 convolution layer) of C5, with the improvements of

2.2 points for the AP^{box} of object detection, and 1.6 points for the AP^{mask} of instance segmentation. Moreover, by inserting DGMN modules into all residual blocks of C4 and C5, we obtain further improvements. Qualitative results of DGMN (C4, C5) and Mask R-CNN are shown in Figure 6. These experiments thus show the effectiveness of our proposed model for learning and refining the deep feature representations in a backbone network.

Computational overhead: fully-connected graphs v.s. DGMN. A key advantage of learning a dynamic graph is that it requires less computation than fully-connected models such as Non-local [48] and still achieve superior performance. This is shown for both the segmentation and detection tasks in Tables 1 and 3 where we outperform Non-local in both accuracy and efficiency (FLOPs and number of parameters). Furthermore, note that one variant of our model, DGMN w/ DA+DW achieves the same performance as Non-local on semantic segmentation on Cityscapes, while the number of FLOPs is only 9.4% and parameters 25.3% of Non-local.

5.3 Comparison to State-of-the-art

Performance on Cityscapes test set. Table 2 compares our approach with state-of-the-art approaches on Cityscapes. Note that all methods are trained using only the fine annotations and evaluated on the public evaluation server as test-set annotations are withheld from the public. As shown in the table, DGMN (ours) achieves an mIoU of 81.8%, surpassing all previous works. Note that we followed common practice and employed several complementary strategies used in semantic segmentation to boost performance, including Online Hard Example Mining (OHEM) [42, 36, 29, 56], Multi-Grid [8, 15, 10] and Multi-Scale (MS) ensembling [6, 9, 58, 56, 13]. The contribution of each strategy on the final performance is reported in the Appendix A. Among competing methods, GloRe [10] and OCNet [56] are the most related to us as they both consider a fully-connected graph. As shown in Table 2, our dynamic graph model achieves better performance while having less computational overhead compared to them.

Performance on COCO 2017 test set. Table 5 presents our results on the COCO test set, where we compare to a strong Mask-RCNN baseline. By inserting DGMN into all layers of C4 and C5, we substantially improve the performance of Mask R-CNN, observing a gain of 3.0 and 2.2 points on the AP^{box} and the AP^{mask} of object detection and instance segmentation respectively. We observe similar improvements when using the ResNet-101 or ResNeXt-101 backbones as well, showing that our proposed DGMN module generalises to multiple backbone architectures.

6 Conclusion

We have proposed Dynamic Graph Message Passing Networks, a novel graph neural network module that dynamically determines the graph structure for each input. It adaptively samples a small set of relevant neighbours for each node, and also predicts the weights and affinity matrix used to propagate information through this sampled neighbourhood. This formulation significantly reduce the computation cost of static, fully-connected graphs such as Non-local networks [48] which contain many redundancies. This is exhibited by the fact that we are able to improve upon the accuracy of Non-local, and several state-of-art baselines, on three complex computer vision problems.

Acknowledgement This work is supported by EPSRC Programme Grant Seebibyte EP/M013774/1. The authors would like to thank Jiarui Xu, Yi Zhu, Shuyang Sun and Kaiyang Zhou for valuable discussions and providing computing resources.

A Further analysis

Effectiveness of different training and inference strategies. To boost the performance on Cityscapes, we followed common practice and employed several complementary strategies used in semantic segmentation, including Online Hard Example Mining (OHEM) [42, 36, 29, 56, 53], Multi-Grid [8, 15, 10] and Multi-Scale (MS) ensembling [6, 9, 58, 56, 13]. The contribution of each strategy is reported in Table 6.

Effectiveness of different sampling rate φ and group of predicted weights G (Section 3.3 and 3.4 in main paper). For our experiments on Cityscapes, where are network has a stride of 8, the sampling rates are set to $\varphi = \{1, 6, 12, 24, 36\}$. For experiments on COCO, where the network stride is 32, we use smaller sampling rates of $\varphi = \{1, 4, 8, 12\}$ in C5. We keep the same sampling rate in

C4 when DGMN modules are inserted into C4 as well. Without otherwise stated, we use $G = 4$ as default. Each group of C/G feature channels shares the same set of filter parameters [11]. The effect of different sampling rate and group of predicted filter weights are studied in Table 7 and Table 8.

Table 6: Ablation studies of different training and inference strategies. Our method (DGMN w/ DA+DW+US) is evaluated under single scale mIoU with ResNet-101 backbone on Cityscapes validation set.

	OHEM	Multi-grid	MS	mIoU (%)
FCN w/ DGMN	✗	✗	✗	79.2
FCN w/ DGMN	✓	✗	✗	79.7
FCN w/ DGMN	✓	✓	✗	80.3
FCN w/ DGMN	✓	✓	✓	81.1

Table 7: Quantitative analysis on different sampling rate of our dynamic sampling strategy in the proposed DGMN model on the Cityscapes validation set. We use a ResNet-101 as backbone. All methods are evaluated on the single scale mIoU.

	DA	DW	US	RWS	mIoU (%)
Dilated FCN	✗	✗	✗	✗	75.0
+ DGMN ($\varphi = \{1\}$)	✓	✗	✗	✗	76.5
+ DGMN ($\varphi = \{1\}$)	✓	✓	✗	✗	79.1
+ DGMN ($\varphi = \{1, 1, 1, 1, 1\}$)	✓	✓	✓	✗	79.2
+ DGMN ($\varphi = \{1, 6, 12\}$)	✓	✓	✓	✗	79.7
+ DGMN ($\varphi = \{1, 6, 12, 24, 36\}$)	✓	✓	✓	✗	80.3
+ DGMN ($\varphi = \{1, 6, 12, 24, 36\}$)	✓	✓	✗	✓	80.4

Table 8: Quantitative analysis on different group number and sampling rate of the proposed DGMN model on the COCO 2017 validation set. All methods are based on the Mask R-CNN detection pipeline with ResNet-50 backbone. Modules are inserted after all the 3×3 convolution layers of C5 (*res5*) of ResNet-50.

	DA	DW	US	RWS	AP ^{box}	AP ^{mask}
Mask R-CNN [34, 18]	✗	✗	✗	✗	37.8	34.4
+ DGMN ($\varphi = \{1, 4, 8, 12\}, G = 0$)	✓	✗	✗	✗	39.4	35.6
+ DGMN ($\varphi = \{1, 4, 8, 12\}, G = 0$)	✓	✗	✗	✓	39.9	35.9
+ DGMN ($\varphi = \{1, 4, 8\}, G = 2$)	✓	✓	✗	✓	39.5	35.6
+ DGMN ($\varphi = \{1, 4, 8\}, G = 4$)	✓	✓	✗	✓	39.8	35.9
+ DGMN ($\varphi = \{1, 4, 8, 12\}, G = 4$)	✓	✓	✗	✓	40.0	36.0

Effectiveness of feature learning with DGMN on stronger backbones. We insert DGMN into deeper and more powerful backbone networks, such as ResNet 101 and ResNeXt 101 [19, 50]. These results are shown in Table 9. By inserting DGMN at the convolutional stage C5 of ResNet-101, DGMN (C5) outperforms the Mask R-CNN baseline with 1.6 points on the metric AP^{box} and 1.2 points on the metric AP^{mask}. On ResNeXt-101, DGMN (C5) also improves by 1.5 and 0.9 points on the AP^{box} and the AP^{mask}, respectively.

Table 9: Quantitative results via applying the proposed DGMN module into different strong backbone networks for object detection and instance segmentation on COCO 2017 validation set.

Model	Backbone	AP ^{box}	AP ₅₀ ^{box}	AP ₇₅ ^{box}	AP ^{mask}	AP ₅₀ ^{mask}	AP ₇₅ ^{mask}
Mask R-CNN [34, 18] + DGMN (C5)	ResNet-101	40.1 41.7	61.7 63.8	44.0 45.7	36.2 37.4	58.1 60.4	38.3 39.8
Mask R-CNN [34, 18] + DGMN (C5)	ResNeXt-101	42.2 43.7	63.9 65.9	46.1 47.8	37.8 38.7	60.5 62.1	40.2 41.3

References

- [1] D. Bahdanau, K. Cho, and Y. Bengio. Neural machine translation by jointly learning to align and translate. In *ICLR*, 2015.
- [2] P. Battaglia, R. Pascanu, M. Lai, D. J. Rezende, et al. Interaction networks for learning about objects, relations and physics. In *NeurIPS*, 2016.
- [3] P. W. Battaglia, J. B. Hamrick, V. Bapst, A. Sanchez-Gonzalez, V. Zambaldi, M. Malinowski, A. Tacchetti, D. Raposo, A. Santoro, R. Faulkner, et al. Relational inductive biases, deep learning, and graph networks. In *arXiv preprint arXiv:1806.01261*, 2018.
- [4] L. Bertinetto, J. F. Henriques, J. Valmadre, P. Torr, and A. Vedaldi. Learning feed-forward one-shot learners. In *NIPS*, 2016.
- [5] J. Bruna, W. Zaremba, A. Szlam, and Y. LeCun. Spectral networks and locally connected networks on graphs. In *ICLR*, 2013.
- [6] L.-C. Chen, G. Papandreou, I. Kokkinos, K. Murphy, and A. L. Yuille. Semantic image segmentation with deep convolutional nets and fully connected CRFs. In *ICLR*, 2015.
- [7] L.-C. Chen, G. Papandreou, I. Kokkinos, K. Murphy, and A. L. Yuille. Deeplab: Semantic image segmentation with deep convolutional nets, atrous convolution, and fully connected crfs. *TPAMI*, 2018.
- [8] L.-C. Chen, G. Papandreou, F. Schroff, and H. Adam. Rethinking atrous convolution for semantic image segmentation. *arXiv preprint arXiv:1706.05587*, 2017.
- [9] L.-C. Chen, Y. Zhu, G. Papandreou, F. Schroff, and H. Adam. Encoder-decoder with atrous separable convolution for semantic image segmentation. In *ECCV*, 2018.
- [10] Y. Chen, M. Rohrbach, Z. Yan, S. Yan, J. Feng, and Y. Kalantidis. Graph-based global reasoning networks. In *CVPR*, 2019.
- [11] F. Chollet. Xception: Deep learning with depthwise separable convolutions. In *CVPR*, 2017.
- [12] M. Cordts, M. Omran, S. Ramos, T. Rehfeld, M. Enzweiler, R. Benenson, U. Franke, S. Roth, and B. Schiele. The cityscapes dataset for semantic urban scene understanding. In *CVPR*, 2016.
- [13] J. Dai, K. He, and J. Sun. Boxesup: Exploiting bounding boxes to supervise convolutional networks for semantic segmentation. In *ICCV*, 2015.
- [14] J. Dai, H. Qi, Y. Xiong, Y. Li, G. Zhang, H. Hu, and Y. Wei. Deformable convolutional networks. In *ICCV*, 2017.
- [15] J. Fu, J. Liu, H. Tian, Z. Fang, and H. Lu. Dual attention network for scene segmentation. In *CVPR*, 2019.
- [16] J. Gilmer, S. S. Schoenholz, P. F. Riley, O. Vinyals, and G. E. Dahl. Neural message passing for quantum chemistry. In *ICML*, 2017.
- [17] W. Hamilton, Z. Ying, and J. Leskovec. Inductive representation learning on large graphs. In *NIPS*, 2017.
- [18] K. He, G. Gkioxari, P. Dollár, and R. Girshick. Mask r-cnn. In *ICCV*, 2017.
- [19] K. He, X. Zhang, S. Ren, and J. Sun. Deep residual learning for image recognition. In *CVPR*, 2016.
- [20] W. Huang, T. Zhang, Y. Rong, and J. Huang. Adaptive sampling towards fast graph representation learning. In *NeurIPS*, 2018.
- [21] Z. Huang, X. Wang, L. Huang, C. Huang, Y. Wei, and W. Liu. Ccnet: Criss-cross attention for semantic segmentation. In *arXiv preprint arXiv:1811.11721*, 2018.
- [22] M. Jaderberg, K. Simonyan, A. Zisserman, and K. Kavukcuoglu. Spatial transformer networks. In *NIPS*, 2015.
- [23] X. Jia, B. De Brabandere, T. Tuytelaars, and L. V. Gool. Dynamic filter networks. In *NeurIPS*, 2016.
- [24] T.-W. Ke, J.-J. Hwang, Z. Liu, and S. X. Yu. Adaptive affinity fields for semantic segmentation. In *ECCV*, 2018.
- [25] T. N. Kipf and M. Welling. Semi-supervised classification with graph convolutional networks. In *ICLR*, 2017.
- [26] S. Kong and C. C. Fowlkes. Recurrent scene parsing with perspective understanding in the loop. In *CVPR*, 2018.
- [27] A. Krizhevsky, I. Sutskever, and G. E. Hinton. ImageNet classification with deep convolutional neural networks. In *NeurIPS*, 2012.
- [28] J. Leskovec and C. Faloutsos. Sampling from large graphs. In *SIGKDD*, 2006.
- [29] Q. Li, A. Arnab, and P. H. Torr. Holistic, instance-level human parsing. In *BMVC*, 2017.
- [30] Y. Li, D. Tarlow, M. Brockschmidt, and R. Zemel. Gated graph sequence neural networks. In *ICLR*, 2015.
- [31] G. Lin, C. Shen, I. Reid, and A. van den Hengel. Deeply learning the messages in message passing inference. In *NeurIPS*, 2015.

- [32] T.-Y. Lin, M. Maire, S. Belongie, J. Hays, P. Perona, D. Ramanan, P. Dollár, and C. L. Zitnick. Microsoft coco: Common objects in context. In *ECCV*, 2014.
- [33] F. Manessi, A. Rozza, and M. Manzo. Dynamic graph convolutional networks. *arXiv preprint arXiv:1704.06199*, 2017.
- [34] F. Massa and R. Girshick. maskrcnn-benchmark: Fast, modular reference implementation of Instance Segmentation and Object Detection algorithms in PyTorch. <https://github.com/facebookresearch/maskrcnn-benchmark>, 2018.
- [35] A. Oliva and A. Torralba. The role of context in object recognition. *Trends in cognitive sciences*, 2007.
- [36] T. Pohlen, A. Hermans, M. Mathias, and B. Leibe. Full-resolution residual networks for semantic segmentation in street scenes. In *CVPR*, 2017.
- [37] A. Rabinovich, A. Vedaldi, C. Galleguillos, E. Wiewiora, and S. Belongie. Objects in context. In *ICCV*, 2007.
- [38] S. Rota Bulò, L. Porzi, and P. Kotschieder. In-place activated batchnorm for memory-optimized training of dnns. In *CVPR*, 2018.
- [39] F. Scarselli, M. Gori, A. C. Tsoi, M. Hagenbuchner, and G. Monfardini. The graph neural network model. *TNNLS*, 2009.
- [40] K. T. Schütt, F. Arbabzadah, S. Chmiela, K. R. Müller, and A. Tkatchenko. Quantum-chemical insights from deep tensor neural networks. *Nature communications*, 2017.
- [41] E. Shelhamer, D. Wang, and T. Darrell. Blurring the line between structure and learning to optimize and adapt receptive fields. *arXiv preprint arXiv:1904.11487*, 2019.
- [42] A. Shrivastava, A. Gupta, and R. Girshick. Training region-based object detectors with online hard example mining. In *CVPR*, 2016.
- [43] M. Simonovsky and N. Komodakis. Dynamic edge-conditioned filters in convolutional neural networks on graphs. In *CVPR*, 2017.
- [44] K. Simonyan and A. Zisserman. Very deep convolutional networks for large-scale image recognition. In *ICLR*, 2015.
- [45] S. Sukhbaatar, J. Weston, R. Fergus, et al. End-to-end memory networks. In *NeurIPS*, 2015.
- [46] A. Vaswani, N. Shazeer, N. Parmar, J. Uszkoreit, L. Jones, A. N. Gomez, Ł. Kaiser, and I. Polosukhin. Attention is all you need. In *NeurIPS*, 2017.
- [47] P. Veličković, G. Cucurull, A. Casanova, A. Romero, P. Lio, and Y. Bengio. Graph attention networks. In *ICLR*, 2018.
- [48] X. Wang, R. Girshick, A. Gupta, and K. He. Non-local neural networks. In *CVPR*, 2018.
- [49] F. Wu, A. Fan, A. Baeviski, Y. N. Dauphin, and M. Auli. Pay less attention with lightweight and dynamic convolutions. In *ICLR*, 2019.
- [50] S. Xie, R. Girshick, P. Dollár, Z. Tu, and K. He. Aggregated residual transformations for deep neural networks. In *CVPR*, 2017.
- [51] D. Xu, W. Ouyang, X. Alameda-Pineda, E. Ricci, X. Wang, and N. Sebe. Learning deep structured multi-scale features using attention-gated crfs for contour prediction. In *NIPS*, 2017.
- [52] M. Yang, K. Yu, C. Zhang, Z. Li, and K. Yang. Denseaspp for semantic segmentation in street scenes. In *CVPR*, 2018.
- [53] C. Yu, J. Wang, C. Peng, C. Gao, G. Yu, and N. Sang. Bisenet: Bilateral segmentation network for real-time semantic segmentation. In *ECCV*, 2018.
- [54] C. Yu, J. Wang, C. Peng, C. Gao, G. Yu, and N. Sang. Learning a discriminative feature network for semantic segmentation. In *CVPR*, 2018.
- [55] F. Yu and V. Koltun. Multi-scale context aggregation by dilated convolutions. In *ICLR*, 2016.
- [56] Y. Yuan and J. Wang. Ocnet: Object context network for scene parsing. *arXiv preprint arXiv:1809.00916*, 2018.
- [57] R. Zhang, S. Tang, Y. Zhang, J. Li, and S. Yan. Scale-adaptive convolutions for scene parsing. In *ICCV*, 2017.
- [58] H. Zhao, J. Shi, X. Qi, X. Wang, and J. Jia. Pyramid scene parsing network. In *CVPR*, 2017.
- [59] H. Zhao, Y. Zhang, S. Liu, J. Shi, C. Change Loy, D. Lin, and J. Jia. Psanet: Point-wise spatial attention network for scene parsing. In *ECCV*, 2018.
- [60] S. Zheng, S. Jayasumana, B. Romera-Paredes, V. Vineet, Z. Su, D. Du, C. Huang, and P. H. S. Torr. Conditional random fields as recurrent neural networks. In *ICCV*, 2015.
- [61] X. Zhu, H. Hu, S. Lin, and J. Dai. Deformable convnets v2: More deformable, better results. In *CVPR*, 2019.